Polymer brush collapse under shear flow

Airidas Korolkovas, Cesar Rodriguez-Emmenegger, Andres de los Santos Pereira, Alexis Chennevière, Frédéric Restagno, Maximilian Wolff, Franz Adlmann, Andrew Dennison, Philipp Gutfreund

Polymer Brush Collapse under Shear Flow

Airidas Korolkovas,[*,†,‡] Cesar Rodriguez-Emmenegger,[§] Andres de los Santos Pereira,[∥] Alexis Chennevière,[⊥] Frédéric Restagno,[#] Maximilian Wolff,[%] Franz A. Adlmann,[%] Andrew J. C. Dennison,[&,†,$] and Philipp Gutfreund[*,†]

[†]Institut Laue-Langevin, 71 rue des Martyrs, 38000 Grenoble, France

[‡]Université Grenoble Alpes, Liphy, 140 Rue de la Physique, 38402 Saint-Martin-d'Hères, France

[§]DWI - Leibniz Institute for Interactive Materials and Institute of Technical and Macromolecular Chemistry, RWTH Aachen University, Forckenbeckstraße 50, 52074 Aachen, Germany

[∥]Institute of Macromolecular Chemistry, Academy of Sciences of the Czech Republic v.v.i., Heyrovsky Sq. 2, 162 06 Prague, Czech Republic

[⊥]Laboratoire Léon Brillouin, CEA, CNRS, Université Paris-Saclay, Saclay, 91191 Gif-sur-Yvette, Cedex, France

[#]Laboratoire de Physique des Solides, CNRS, Univ. Paris-Sud, Université Paris-Saclay, 91405 Orsay, Cedex, France

[%]Division for Material Physics, Department for Physics and Astronomy, Uppsala University, Box 516, 75120 Uppsala, Sweden

[&]Department of Chemistry, Technical University Berlin, 10623 Berlin, Germany

[$]Department of Physics and Astronomy, University of Sheffield, S10 2TN Sheffield, U.K.

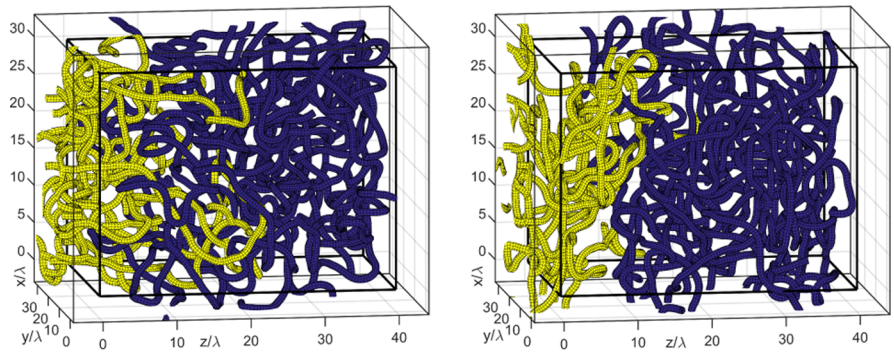

ABSTRACT: Shear responsive surfaces offer potential advances in a number of applications. Surface functionalization using polymer brushes is one route to such properties, particularly in the case of entangled polymers. We report on neutron reflectometry measurements of polymer brushes in entangled polymer solutions performed under controlled shear as well as coarse-grained computer simulations corresponding to these interfaces. Here we show a reversible and reproducible collapse of the brushes, increasing with the shear rate. Using two brushes of greatly different chain lengths and grafting densities, we demonstrate that the dynamics responsible for the structural change of the brush are governed by the free chains in solution rather than the brush itself, within the range of parameters examined. The phenomenon of the brush collapse could find applications in the tailoring of nanosensors and as a way to dynamically control surface friction and adhesion.

INTRODUCTION

A polymer brush is a unique type of surface functionalization, consisting of long polymer chains densely tethered by one end to a surface.[1,2] The conformation of a solvated polymer brush is markedly different to that of chains in bulk polymer solution as the brush must stretch away from the surface to minimize contact with the densely grafted neighboring chains. Polymer brushes have broad interest across a variety of sectors since tuning interfacial properties (e.g., chemical composition, molecular weight, grafting density) can yield surface coatings with a high degree of control and in some cases completely new functionality.

One of the most common uses for brushes is to inhibit protein adsorption and prevent surface fouling.[3,4] Various other applications are also under investigation[5] ranging from bioactive interfaces,[6] to brush-mediated lubrication,[7,8] to soil release in textiles,[9] and even to semiconductor manufacturing.[10,11] Another emerging application is the use of polymer brushes as nanosensors reacting to various stimuli including pressure,[12] light,[13] temperature,[14] and pH,[15] among others.

Remarkably, the sensitivity of these nanoscale sensors can be finely tuned by the amount of the brush swelling,[16] which in turn depends on the nature of the solvent but can also be affected by other factors such as shear stress as will be shown in this article.

The static properties of polymer brushes are well understood thanks to extensive theoretical,[17] computer simulation,[18,19] and experimental[20−23] studies. The knowledge of brush dynamics, however, is still incomplete, even though it is crucial for the design of the aforementioned sensors. To help fill this demand, our study will focus on the response of brushes to an applied shear stress while swollen and deeply interpenetrated with a bulk polymer solution, illustrated in Figure 1. Aside from use in

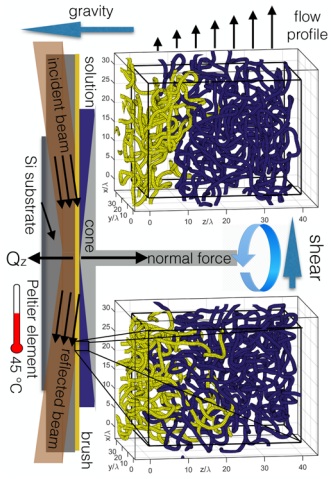

Figure 1. Experimental setup and simulated polymer conformation. The experiments are conducted with the silicon−polymer interface horizontally oriented. The wavevector transfer Q_z is perpendicular to the interface. The temperature of the silicon substrate is controlled by a Peltier element from the bottom side. Shear is applied by the rheometer via a titanium cone or plate. The lower right panel shows a conformation snapshot plotted from the simulation data. The interpenetration of the polymer brush (yellow) and free chains (blue) is clearly visible. With applied shear (upper right panel) the free chains are pulled out of the brush, the mean thickness of the brush decreases, and the interface becomes sharper. The density profiles along the z-direction are compared to the neutron reflectometry data.

sensors, surfaces decorated with brushes may also play a key role to control adhesion,[24,25] lubrication,[26] friction,[27,28] and in microfluidic devices[29] and confined channels.[30] In our experimental conditions, the chains are strongly entangled reaching a relaxation time on the order of $\tau_d = 1$ s, which has immediate practical importance since it can dynamically interact with the flows encountered in the aforementioned real-world applications, which commonly have similar time scales. However, the brush−bulk interface remains very challenging to investigate either theoretically[31] or experimentally due to its complex, heterogeneous, strongly interacting, nonequilibrium, and confined nature. We have therefore taken a two-pronged approach and used a recently developed computer simulation technique[32] as well as state-of-the-art experimental rheology−neutron reflectometry (rheo-NR)[33] capabilities. This combination enables greater insight into what is occurring at the interface compared to the two approaches taken separately.

Simulation of polymer brushes under shear[34,35] is a vibrant field: brushes in good solvent,[36,37] two opposing polyzwitterionic brushes,[38] brushes in contact with short melt chains,[39] and stiff brushes related to biological membranes,[40] just to name a few recent publications. However, most of the simulations (molecular dynamics, dissipative particle dynamics, and various kinds of Monte Carlo) are based on $\lambda \approx 1$ nm size beads running at time steps of about $\tau_m = 10^{-12}$ s, required to follow the thermal fluctuations of the bead momentum. Current computers can typically perform 10^8 time steps within a reasonable execution time; insufficient to bridge the gap to our experimental goal of $\tau_d = 1$ s.

The next level of coarse-graining is the Brownian dynamics where we abandon the bead momentum altogether and only track their positions, which take about $\tau = 10^{-9}$ s to relax after diffusing a distance greater than their own size. This technique has already been used to predict a brush collapse under shear.[41] However, the reported collapse occurred at a shear rate approaching $\dot{\gamma} \approx 1/\tau \approx 10^9$ s^{-1} and was due to the finite extensibility of the polymer backbone. Such extreme shear rates are more akin to an explosion than a well controlled shear experiment, and this mode of brush collapse is not related to the entanglement dynamics at $\dot{\gamma} \approx 1/\tau_d \approx 1$ s^{-1} relevant to realistic flow conditions measured in our study.

Our experiments are done using polystyrene (PS) in a good solvent at $\phi = 30\%$ fraction by weight. To describe this liquid, the appropriate coarse particle is called a blob,[42] and its size corresponds to the typical distance between neighboring polymer chains: $\lambda = a\phi^{-3/4}$, where $a \approx 7$ Å is the size of one styrene monomer. The blob repulsion is best quantified by an effective Gaussian potential which results in the correct static structure.[43] Dynamically, however, this blob potential was considered too weak and too soft to prevent chain crossings[44] and therefore unable to produce any entanglements. A recent study,[32] however, has proposed to smear out the Gaussian potential in both time and space, thus suppressing chain crossings while retaining the long Brownian time step τ adequate to describe our experiments.

Neutron reflectometry (NR) is a powerful experimental tool for the structural and dynamical investigation of polymer brushes, thanks to the possibility of isotopic replacement to enhance the contrast between the grafted and the bulk polymers, as well as its atomic resolution and noninvasive nature. A unique advantage of NR is that most engineering materials like aluminum or silicon are transparent for the neutrons which permits direct measurement of the brush−bulk interface through the silicon substrate.[33] Structural investigations of brushes under shear load have been performed by NR measurements on PS brushes in solvents[45,46] but found no measurable effect. Next, we look at two studies which examined a PS brush in contact with a PS melt. The first one was measured *in situ* while shearing.[47] No reproducible result could be obtained, and it was explained by metastable states of the brush. However, very high torques were applied in that study, and the brushes were not characterized after the shear experiments. It has been shown by NR that PS brushes can be destroyed by high torque shear,[48] and such a scenario is likely in the aforementioned experiment. The second study also sheared PS brushes in a PS melt,[49] which were then rapidly quenched below their glass transition temperature and measured *ex situ* with NR, reporting a reproducible retraction of the brush. In our present study we have used NR for an *in situ* characterization of the behavior of PS brushes under shear by an entangled PS solution in diethyl phthalate (DEP, a good solvent of very low volatility). The use of solution rather than

melt is more relevant to biological processes as well as microfluidic applications.

Here we show both experimentally and computationally that the entangled polymer brush thickness decreases with shear. More precisely, we observe a shrinking of brushes proportional to the square of the applied shear rate. This nonlinear effect is attributed to the normal stress difference, which is an excess pressure buildup perpendicular to the applied shear flow, and is well-known to occur in bulk entangled polymer fluids, where it leads to the so-called Weissenberg effect.[50] The time scale of the brush collapse is determined by the reptation time of the free chains in solution, rather than the internal dynamics of the brush. The brush thickness returns to equilibrium upon cessation of shear, and the effect can by cycled many times over. The experimental and simulation findings are in good agreement and are further corroborated by a simple phenomenological theory.

EXPERIMENTAL SECTION

Materials. *N*,*N*,*N*′,*N*″,*N*″-Pentamethyldiethylenetriamine (PMDETA, 99%), styrene (99%), diethoxy(3-glycidyloxypropyl)methysilane (99%), dichloromethane (99%), and diethyl phthalate (DEP) (99%) were purchased from Sigma-Aldrich (Czech Republic). Deuterated polystyrene (dPS), M_w = 627 kg mol^{-1}, M_w/M_n = 1.09, correspopnding to $P = M_w/112.2$ g mol^{-1} = 5570, was purchased from Polymer Source, Canada. Monocrystalline silicon blocks of size 7 × 7 × 1 cm, orientation (1, 0, 0), were purchased from CrysTec, Germany. Styrene was distilled over CaH_2 under reduced pressure and stored under Ar.

[11-(2-Bromo-2-methyl)propionyloxy]undecyltrichlorosilane was synthesized according to a previously published protocol.[51]

Preparation of Brush Long-Sparse: "Grafting-To" Approach. The amino end-functionalized PS was synthesized in-house to a molecular weight of M_n = 218 kg/mol ($N = M_n/104.15$ g mol^{-1} = 2093) and a polydispersity of 1.23. Then it was grafted onto a self-assembled monolayer (SAM) of diethoxy(3-glycidyloxypropyl)-methysilane) deposited on a single crystal silicon block. Details about the sample preparation can be found in ref 52. The thickness of the SAMs was determined by ellipsometry and found to be 1.0 nm for both brushes corresponding to fully stretched and upright standing chains in accord with previous samples.[52] The silicon oxide thickness was determined by NR as described in the Supporting Information.

Preparation of Brush Short-Dense: "Grafting-From" Approach. PS brushes were grafted from an initiator-coated substrate by surface-initiated atom transfer radical polymerization (ATRP) employing a literature procedure,[53] modified to achieve a lower grafting density and high thickness. First, a self-assembled monolayer of ATRP initiator was immobilized on the surface. The substrate (silicon slab) was rinsed with toluene, acetone, ethanol, and deionized water, blown dry with nitrogen, and activated in a UV/O_3 cleaner for 20 min. Without delay, the sample was placed in a custom-made reactor vessel, which was then sealed, evacuated, and refilled with Ar. A 1 μg mL^{-1} solution of (11-(2-bromo-2-methyl)propionyloxy)undecyl-trichlorosilane in anhydrous toluene was added until the sample was fully immersed. The immobilization of the initiator was allowed to proceed for 3 h at room temperature, and the sample was subsequently removed from the reactor, rinsed copiously with toluene, acetone, ethanol, and deionized water, and dried by blowing with nitrogen.

To achieve a lowered grafting density, a fraction of the surface-grafted ATRP initiator groups were deactivated by nucleophilic substitution with NaN_3. The sample was placed in a custom-made reactor, which was then sealed, evacuated, and refilled with Ar, and placed in a thermostatic bath at 60 °C for 1 h to reach thermal equilibrium. A solution of NaN_3 (3.4 mg mL^{-1}) in anhydrous *N*,*N*-dimethylformamide (DMF), previously heated to 60 °C, was added to completely cover the sample, and the reaction was allowed to proceed at 60 °C for 8 h. Subsequently, the reaction was stopped by replacing the solution in the reactor with pure DMF. The sample was removed from the reactor, rinsed copiously with DMF, ethanol, and deionized water, and dried by carefully blowing with nitrogen.

For the surface-initiated ATRP, styrene (40 mL, 349 mmol), anhydrous toluene (20 mL), and PMDETA (760 μL, 3.64 mmol) were degassed in Schlenk flask via three freeze−pump−thaw cycles. The solution was transferred under Ar to another Schlenk flask containing CuBr (496 mg, 3.46 mmol) and $CuBr_2$ (40 mg, 0.179 mmol), which had been previously deoxygenated by three vacuum/Ar-backfilling cycles. The flask containing the polymerization solution was placed in thermostatic bath at 90 °C and stirred vigorously for 1 h. The initiator-functionalized substrate was placed vertically in a custom-made reactor, which was subsequently closed, deoxygenated by three cycles of vacuum/Ar-backfilling, and placed in a thermostatic oil bath at 90 °C to allow the temperature to equilibrate. The polymerization solution was transferred under Ar to the reactor containing the substrate and the reaction was allowed to proceed at 90 °C for 22 h. The reaction was stopped by opening the reactor and adding toluene, and the substrate was rinsed copiously with toluene, acetone, ethanol, and deionized water and dried by blowing with nitrogen. The dry thickness of the layers was measured by spectroscopic ellipsometry and NR.

Rheology. Deuterated polystyrene (dPS, 0.3 g) was mixed at 30% weight fraction with diethyl phthalate (DEP, 0.7 g, a good solvent of low volatility) in a round-bottom flask. It was topped with an abundant amount (50 mL) of dichloromethane (also a good solvent, but high volatility) and stirred for several hours to fully dissolve the dPS. The dichloromethane was then slowly removed in a rotary evaporator under reduced pressure, which ensured that no gas bubbles were left trapped in the resulting viscous liquid.

A Teflon spatula was used to transfer the dPS-DEP solution onto the brush-coated silicon crystal. The liquid was then contained in an Anton-Paar MCR 501 rheometer in cone−plate or plate−plate geometry (1° cone angle, 50 mm diameter for cone or plate) to allow *in situ* rheology as explained in ref 33. The rotating cone or plate on top was made of titanium, and its surface was sand-blasted to reduce surface slip at the moving interface. The temperature on the stationary brush-coated side was kept constant at 45 °C throughout the experiment.

Neutron Experiment Details. Neutron reflectometry was carried out on FIGARO at the Institut Laue-Langevin, Grenoble, France.[54] The measurements were performed in time-of-flight mode using a wavelength band from 2.2−21 Å and a wavelength resolution of 7%. Two reflection angles (0.62° and 2.72°) were used to cover the full *Q*-range by rotating the incident beam and the detector around the sample keeping the rheometer horizontal at all times. The relative angular divergence was set to $\Delta\theta/\theta$ = 1.5% for both reflection angles. The acquisition time was 1−5 min for the first reflection angle and 25 min for the second angle, and all measurements under shear were reproduced and cycled several times to exclude any transient phenomena. The footprint of the neutron beam (39 × 35 mm^2) was centered to the cone/plate; hence, the scattering momentum transfer is parallel to the shear gradient. The rheo-NR setup with the neutrons entering through the side of the stationary silicon substrate (see Figure 1) is explained in more detail in ref 33.

SIMULATION METHOD

Each chain is described by a continuous path $\mathbf{R}(s)$ where $s \in (0, 1)$ is the monomer label. The chains have N degrees of freedom and repel one another via a Gaussian potential $\Phi(\mathbf{r}) = k_BTe^{-\mathbf{r}^2/(2\lambda^2)}$, while the backbone stays connected via a harmonic spring interaction of the same strength k_BT and the same length λ. The continuous backbone s is sampled by a number of $J = 4N$ discrete points:

$$\mathbf{R}_j = \mathbf{a}_0 + 2\sum_{n=1}^{N-1} \mathbf{a}_n \cos\left(\frac{\pi(2j-1)n}{2J}\right) \quad (1)$$

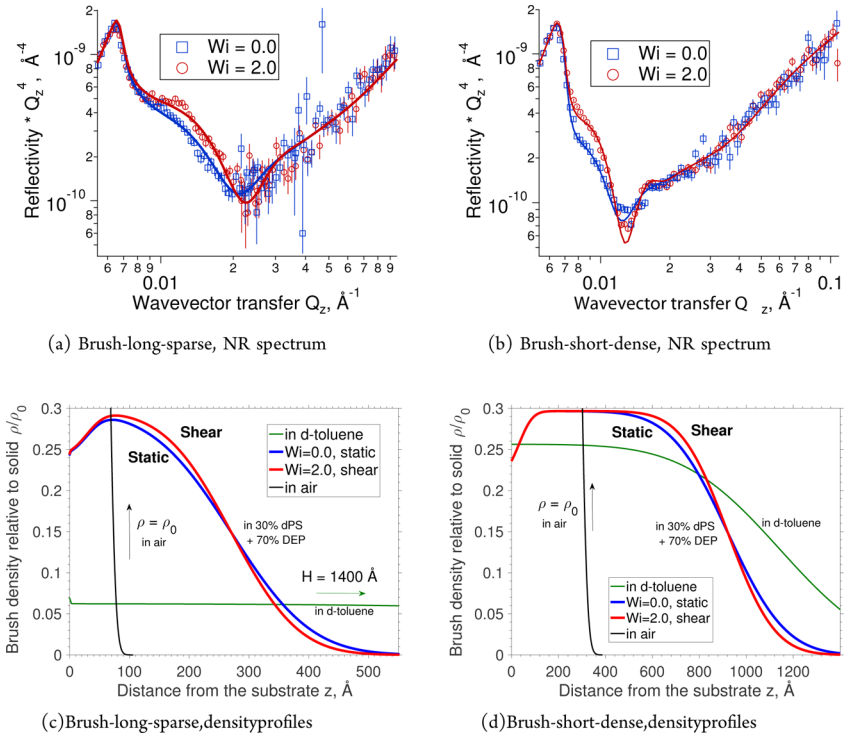

(a) Brush-long-sparse, NR spectrum (b) Brush-short-dense, NR spectrum

(c)Brush-long-sparse,densityprofiles (d)Brush-short-dense,densityprofiles

Figure 2. Experimentally determined brush structure. Panels a and b show NR data (points) and the fits (solid lines) for the two brushes in solution of 30% dPS and 70% DEP. Panels c and d show the corresponding fitted brush density profiles (thick lines) as well as additional fits of NR measurements in air (fully collapsed) and in deuterated toluene (fully stretched). The profiles in air and *d*-toluene emphasize the differences between the static structure of the two brushes, whereas the relative effect of shear is about the same for both samples.

which ensures that neighboring points $|\mathbf{R}_j - \mathbf{R}_{j+1}| \ll \lambda$ are closer together than the potential range of the blob λ, and hence there are effectively no gaps through which the chains could cross. The propagation in time is carried out in terms of N Rouse modes:

$$\mathbf{a}_n(t + \Delta t) = \mathbf{a}_n(t) + (\mathbf{F}_{\text{spring}} + \mathbf{F}_{\text{exvol}})\Delta t + \lambda\sqrt{6\Delta t/(\tau M)}\,\mathcal{R}_n \tag{2}$$

where standard formulas are used to evaluate the spring and the excluded volume forces. The Brownian time unit can be estimated by the Einstein−Stokes formula:

$$\tau = \frac{6\pi\eta_s\lambda^3}{k_B T} \approx 10^{-9}\ \text{s} \tag{3}$$

where $\eta_s = 1.7 \times 10^{-2}$ Pa·s is the viscosity of DEP.

The important novelty in this simulation is that its time resolution is deliberately truncated by updating the random vector $\mathcal{R}_n$ only at intervals of $M = 120$ steps instead of every single $M = 1$ step. This ensures that the random force strength is much weaker than the excluded volume one (by a factor of $\sqrt{M}$), thereby suppressing any chances of chain crossings and giving rise to entanglement dynamics.

Here we note that the maximum applicable shear rate is also limited to about $\dot{\gamma}(M\tau) \ll 1$, and the fastest one we have used was $\text{Wi} = \dot{\gamma}\tau_d = 50$. This leaves us with a safety margin of $1/(M\dot{\gamma}\tau) = 17$, so we do not expect too many chain crossings. Either way, this shear rate is already an order of magnitude faster than the experimental one, leaving us plenty of room for comparison with the experimental data.

In the simulation we did not reconstruct a one-to-one correspondence with either of the experimental brushes. Instead, the simulated brush density was deliberately chosen to be smaller than the experimental one because of two reasons. First, the experimental samples, especially the brush-short-dense, are mostly composed of the "dry" interior region, which would consume a lot of computing time to simulate, without resulting in any interesting effects under shear. Second, a dry and strongly stretched brush cannot be described using the same blob potential as the bulk chains. Instead, smaller blobs must be used[55] to ensure incompressibility which requires the total polymer density to be constant across the whole box (see Figure 4a). Also, the brush blob size would have to shrink further as the brush collapses under shear. This introduces another complication into an already difficult system, whereas we prefer to present the absolutely simplest possible model.

Confinement. To confine the system between two walls, we have used the recently developed mirror-and-shift boundary conditions.[56] Briefly, the entire system is mirrored around the $z = 0$ plane and shifted by half the box length along the other two dimensions. The original system together with its mirror-shifted image is then periodically replicated in all three directions as usual, and all particles interact with their neighbors in the standard way. In other words, every particle interacts with every other particle as well as its mirror-and-shifted images.

At this point we have a perfectly homogeneous system, and the only force driving the particles across the boundaries is the thermal noise of strength $1/\sqrt{M} \ll 1$. To block this and create the actual walls, a soft repulsive potential

$$U(z) = 0.05 k_B T e^{-z/(2\lambda)} \tag{4}$$

is applied on both sides. The range corresponds to the diameter of one blob, while the amplitude is adjusted so that the particle density in the middle of the box is equal to one. The resulting confinement force is comparatively weak and therefore is

perceived as a small perturbation to an otherwise homogeneous system. The coveted result is that the particle density (Figure 4a) goes monotonically from zero outside the box, to one inside the box, without any overshoot or density oscillations. The wall roughness barely exceeds one blob diameter and is about as sharp as possible. The monotonic density climb is in agreement with all of our NR measurements which strongly rule out the possibility of pronounced density oscillations near the surface.

Grafting and Shear. To create a brush, we first generate the locations of the grafting points. For simplicity, they are arranged on a square lattice on the $z = 0$ plane, plus one random number of variance λ in all directions to make it more realistic. To "graft" a chain, we simply add an attractive potential between the grafting point and the central $j = J/2$ monomer:

$$U_{\text{graft}}(\mathbf{r}) = k_{\text{B}}T \cosh(r/\lambda) \tag{5}$$

Half of the grafted chain $j > J/2$ is assigned to the main box and feels the same confinement potential, eq 4, as all the free chains. The other half $j < J/2$ is assigned to the mirrored box and feels the mirrored confinement $U(-z)$. This "grafting" technique is further explained in ref 56. In essence, at our coarse scale it is rather important to attach the central monomer and thread the chain halfway through the wall, instead of the more obvious attachment of a chain end, since this would leave a gap between the confining wall and the grafting point, and then the free chains would have a chance to unphysically cross through that gap.

In terms of traditional end-grafted chains, our bristles have an effective length $N = 256/2 = 128$, and there are $B = 2 \times 8 = 16$ of them. The chain length ratio was kept to $P/N = 2$ for simplicity and is similar to the brush long-sparse experimental situation where the ratio is about 3. The grafting density was 0.006 bristles per $\lambda^2 = (a\phi^{-3/4})^2$. This is about 16 times sparser than the experimental brush long-sparse system, but it was chosen on purpose to leave more empty space in which the brush could collapse under a broad range of shear rates and therefore explore a wider range of conditions than possible experimentally.

The shear flow is generated by adding a Couette velocity profile:

$$\mathbf{v}_{\text{shear}} = \dot{\gamma}|z|\hat{\mathbf{x}} \tag{6}$$

The profile is mirrored across the $z = 0$ plane, so that the $j < J/2$ particles of the grafted chains also feel the shear flow in the correct direction. No slippage or shear bands were assumed and could not easily occur in our simulation due to the phenomenologically imposed shear flow profile. A more realistic model could better assume a constant shear stress and let the velocity profile develop instead, but we have not attempted such a simulation.

RESULTS

Our main experimental result is shown in Figure 2. The applied shear rate $\dot{\gamma}$ is given in dimensionless Weissenberg number

$$\text{Wi} = \dot{\gamma}\tau_{\text{d}} \tag{7}$$

normalized to the longest relaxation time τ_{d} of the bulk liquid which was measured by oscillatory rheology (see Supporting Information Figure 7). The rheo-NR experiment was performed with two brushes prepared by different chemical methods which gave large differences in grafting density and molecular weight, summarized in Table 1: "grafting to" produced a long, sparsely grafted brush (brush long-sparse, or brush-LS) while "grafting from" gave a shorter, denser brush (brush short-dense, or brush-SD). The polymer solution was the same in both cases, ϕ = 30% dPS in 70% DEP. The NR spectrum is displayed in panels a and b, showing an increase of 50% in the reflected intensity between the static and the sheared brush. It is a strong and direct indication that the brush−bulk interface becomes sharper upon shearing. The shear was cycled on and off multiple times to demonstrate that the effect is reversible and reproducible (see Supporting Information Figure 4).

Table 1. Summary of Experimental NR Results

	brush-LS	brush-SD
chain length N	2093	808
grafting density σ	0.016	0.16
H = mean thickness (slab model), Å		
in air	89	333
in *d*-toluene	1400	1167
in 30% dPS, 70% DEP	278	958
h = brush−bulk roughness (Gaussian), Å		
Wi = 0.0 (static)	105	194
Wi = 0.5		191
Wi = 1.0	96	
Wi = 2.0	88	157

To quantify the effect more precisely, we have fitted the data (solid lines in panels a and b) and revealed the actual brush structure in panels c and d, respectively. The model used for the fit was verified to be consistent with information obtained by further complementary measurements, namely the NR spectrum of the brush in air (dry, fully collapsed brush), as well as in a good solvent (maximally swollen brush) which in our case was deuterated toluene. These spectra and details about fitting are available in the Supporting Information.

The main difference between the two brushes is their grafting density σ, defined as the number B of chains per substrate area A, normalized by the monomer size of an effective value a = 7 Å as given in ref 57:

$$\sigma = \frac{Ba^2}{A} \tag{8}$$

Experimentally, this is obtained by measuring the dry brush thickness in air

$$H_{\text{air}} = a\sigma N \tag{9}$$

where N is the number of monomers per grafted chain. In the case of the "grafting-from" brush, we do not know N and σ separately. Therefore, the brush is further characterized by immersing it in a good solvent (deuterated toluene at 20 °C), so the brush swells to a height[58]

$$H_{\text{good solvent}} = aNP^{-1/3}\sigma^{1/3} \tag{10}$$

where $P = 1$ is the length of the free chains, in this case just a single solvent molecule. The dimensionless surface coverage can then be estimated by

$$\sigma = \left(\frac{H_{\text{air}}}{H_{\text{good solvent}}}\right)^{3/2} \tag{11}$$

comparing the dry brush thickness in air versus the thickness in a good solvent. The estimate of σ from eq 11 is valid for the brushes presented here; however, it should be noted that the theoretical scaling law 3/2 may not be exactly obeyed in general, especially for very low density brushes (mushrooms) or very short chains.

The summary of the brush properties determined by NR is listed in Table 1. There is a factor of σ_{SD}/σ_{LS} = 10 difference between the grafting densities of the two brushes as well as a factor of N_{SD}/N_{LS} = 0.4 difference in chain length. One can better appreciate these numbers by comparing how far the brush-LS swells in toluene (a good solvent), with respect to a more modest relative swelling of the brush-SD, as shown in Figures 2c and 2d. When immersed in a 30% homopolymer solution, as opposed to a pure solvent, the excluded volume repulsion between the bristles is partially screened and the brush shrinks considerably, but is still much more swollen than the brush in air. In solution, the density profiles show two regions: (1) an interior region close to the wall where the free chains are almost completely expelled and (2) an overlap region further out where the grafted and free chains overlap and interpenetrate.

Despite the fact that the two brushes are different, the relative effect of shear on both seems to be similar and is restricted to the overlap region. In the case of brush-SD, its wide interior region is not affected by shear at all. Therefore, to quantify the relative change in brush structure under shear, we propose to focus on where the effect occurs and use only the mean thickness of the overlap region, which for simplicity we describe by a triangular shape

$$\rho(z) = \phi\left(1 - \frac{z}{h}\right), \quad 0 < z < h \tag{12}$$

and therefore its mean thickness

$$\langle z \rangle = \frac{\int z\rho \, dz}{\int \rho \, dz} = h/3 \tag{13}$$

is simply proportional to the brush−bulk roughness h and does not involve the full brush thickness H. The relative change in the overlap thickness

$$\frac{\langle z(\mathrm{Wi}) \rangle}{\langle z(0) \rangle} \equiv \frac{h(\mathrm{Wi})}{h(0)} \tag{14}$$

as a function of the applied shear is plotted in Figure 3. Clearly, in these reduced units both brushes seem to follow a universal behavior, within the accessible parameter range.

To better understand the brush collapse, a series of computer simulations were performed using a previously reported algorithm for entangled polymer solutions in bulk,[32] here extended for confined brush−bulk systems under shear flow. We have chosen one set of reasonable parameters resembling the "grafting-to", or brush-LS, sample and have only varied the applied shear rate. In total, we have used C = 64 free chains of length P = 256 in contact with a brush containing B = 16 grafted chains of length N = 128. An entanglement length of N_e = 59 was reported in the original study,[32] obtained using primitive path analysis,[59] leading to $Z = P/N_e$ = 4.3 entanglements per chain in the bulk. The box volume is set fixed to

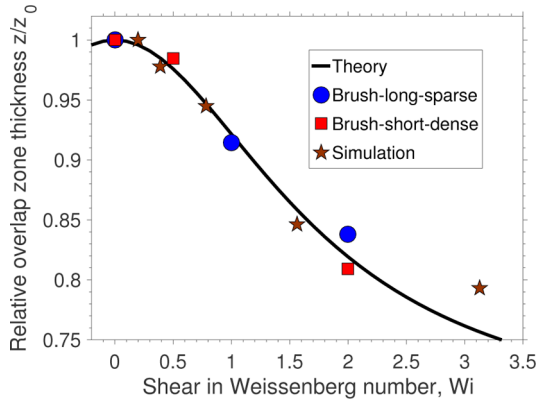

Figure 3. Brush thickness under shear, normalized to the equilibrium thickness. Only the brush−bulk overlap region is considered in this comparison. The fit (solid line) is made using eq 21.

$$V = 2\left(\frac{4\pi}{3}\right)\lambda^3(CP + BN) \tag{15}$$

and its aspect ratio is adjusted so that the grafted chains stay far away from the opposite side of the box. To visualize the system, a smaller version was also simulated and the resulting polymer conformations were plotted in 3D, shown as insets in Figure 1.

Every simulated degree of freedom corresponds to one "blob", which can be mapped to the experimental system using a scaling law[42]

$$N_{\mathrm{blobs}} = \phi^{5/4} N_{\mathrm{monomers}} \tag{16}$$

Equation 16 is a theoretical prediction for an ideal semidilute solution, up to a numerical prefactor of order one. It may require a correction if the solution is too concentrated $\phi \to 1$, which is likely for our experiment. In any case, we have made no attempt to establish an absolute one-to-one correspondence between simulation and experiment and will content ourselves by comparing only the relative change of the brush structure as a function of the dimensionless Weissenberg number, as shown in Figure 3.

One advantage of simulation is that we can explore a much wider range of shear rates than possible experimentally. A shortcoming is that the computation time grows very rapidly $t \propto Z^{4.5}$ (or $t \propto Z^{3.5}$ + overhead for parallel implementations) with the number of entanglements Z, and systems bigger than $Z > 10$ are not very practical. Keeping these considerations in mind, we simulate a lower grafting density, σ_{Sim} = 0.006 bristles per λ^2, in comparison to σ_{LS} = 0.016 per $a^2 = (\lambda\phi^{3/4})^2$ for the experimental brush-LS system. The simulated brush is thus fully overlapping with the bulk, and we do not waste precious computer time to simulate any interior region which is not crucial for the brush collapse to occur. A broad range of shear rates could then be easily examined, ranging from Wi = 0.2 to Wi = 50. The resulting density profiles are shown in Figure 4a, where the blob density is normalized to the number of blobs in the box (eq 15). Each blob contains a ϕ percentage of polymer and $(1 - \phi)$ percentage of solvent as mapped out by eq 16. The simulated density profile can be compared with the experimental one in Figure 2c. Even though there is a roughly $\phi^{-3/2}\sigma_{LS}/\sigma_{\mathrm{Sim}}$ = 16-fold difference in the grafting density and about $\phi^{5/4}N_{LS}/N_{\mathrm{Sim}}$ = 3.6 times difference in the chain length, the overall shape of the brush density profile and its change upon shear seem to be qualitatively similar.

DOI: 10.1021/acs.macromol.6b02525
Macromolecules 2017, 50, 1215−1224

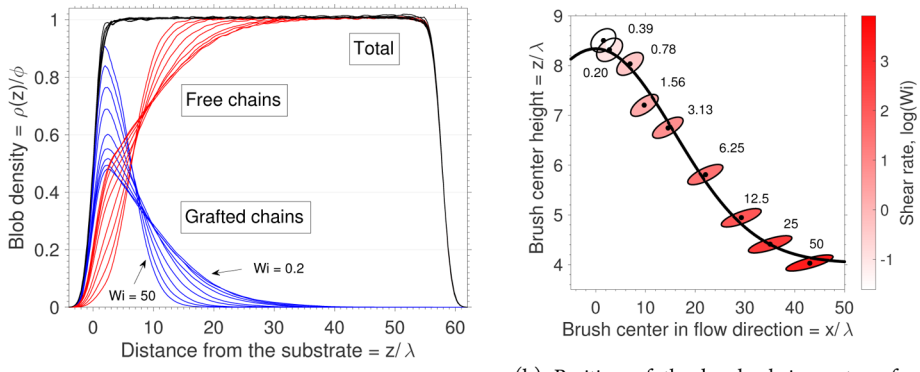

(a) Density profiles under various shear rates given in Weissenberg number $\mathrm{Wi} = \dot{\gamma}\tau_d = 50/2^{1,2,\ldots,9}$.

(b) Position of the brush chain centre of mass relative to its grafting point, as defined in Eq. (17). Ellipses show the radius of gyration scaled to the x-axis (see SI).

Figure 4. Simulated brush structure under shear flow.

For a more quantitative comparison, we have used the definition in eq 13 to calculate the mean thickness of the simulated brush and plotted the value normalized to equilibrium in Figure 3. When compared in terms of reduced units, there emerges a single unified trendline between the simulation and the two experiments, suggesting a common mechanism for shear-induced brush collapse in conditions where the bulk solute is entangled with the brush. Currently, we are not aware of any theoretical description which could calculate the observed brush density profiles (experimental Figure 2c,d and simulation Figure 4a). A scaling law analysis has earlier been reported[60] which roughly quantifies the brush deformation along the shear flow, but it was only intended for short, unentangled chains in which case there is no normal stress difference and hence no change in brush thickness.

Here we continue in the same scaling law spirit and propose a phenomenological explanation of our entangled brush system. At equilibrium, each bristle has a density profile $\rho(x,z)$ around its grafting point. For simplicity, we will restrict ourselves to two dimensions with the z-direction perpendicular to the interface and the flow direction x. Our data indicate (Figure 2d) that the interior region of the brush (if present) is not affected by shear flow, and therefore we will only focus on the overlap region, where the effect takes place. Its center of mass at zero shear is located at

$$\langle x\rangle_0 = \frac{\int x\rho \,\mathrm{d}x\,\mathrm{d}z}{\int \rho \,\mathrm{d}x\,\mathrm{d}z} = 0 \tag{17a}$$

$$\langle z\rangle_0 = \frac{\int z\rho \,\mathrm{d}x\,\mathrm{d}z}{\int \rho \,\mathrm{d}x\,\mathrm{d}z} \approx h \tag{17b}$$

where h denotes the overlap region thickness. Under a steady shear flow, the center of mass moves to some different location $\langle x, z\rangle$. If the shear rate is very small, one can assume phenomenologically that the displacement along the flow $\langle x\rangle$ is linearly proportional to the shear rate (see Supporting Information Figure 9) and to the overlap thickness:

$$\langle x\rangle = (\dot{\gamma}\tau_d)\langle z\rangle \tag{18}$$

where τ_d is the brush–bulk relaxation time, presumably governed by reptation: $\tau_d \approx \tau(P/N_e)^3 \approx 10^5\tau$, for the simulated case. The energy penalty of the deformed brush can be estimated by

$$E/k_BT = \langle x - x_0\rangle^2 + \langle z - z_0\rangle^2 = (\dot{\gamma}\tau_d\langle z\rangle)^2 + \langle z - z_0\rangle^2 \tag{19}$$

A nonlinear fluid such as ours exhibits normal stress differences and hence has a mechanism to couple the stress along various axes. The brush will therefore seek an energy minimum which can be found by solving $\mathrm{d}E/\mathrm{d}\langle z\rangle = 0$, resulting in

$$\langle x\rangle = \left(\frac{\dot{\gamma}\tau_d}{1 + (\dot{\gamma}\tau_d)^2}\right)\langle z\rangle_0 \tag{20a}$$

$$\langle z\rangle = \frac{\langle z\rangle_0}{1 + (\dot{\gamma}\tau_d)^2} \tag{20b}$$

This reasoning shows that the overall chain deformation will be smallest if the overlap thickness $\langle z\rangle$ shrinks below its equilibrium value, thereby avoiding some of the friction from the free chains flowing by. Of course, the brush cannot shrink to zero height and will have to saturate to no thinner than its dry state. The simplest modification could be

$$\frac{\langle z\rangle}{\langle z\rangle_0} = \frac{1-\alpha}{1 + (\beta\dot{\gamma}\tau_d)^2} + \alpha \tag{21}$$

with fitting parameters $\alpha = 0.68$ and $\beta = 0.57$, used to fit the trend in Figure 3.

Another great advantage of simulations is that we gain access to practically any quantity or correlation of interest, including for instance the brush center-of-mass displacement along the flow, $\langle x\rangle$, which is unavailable experimentally. We have plotted the simulated height $\langle z\rangle$ as a function of $\langle x\rangle$ for various shear rates in Figure 4b. In this plot both axes refer to distances, and therefore we could additionally superimpose the ellipses of inertia showing the radius of gyration of the grafted chains around their respective center of mass (more details can be found in the Supporting Information). The ellipses show that not only is the brush displaced, but it is also deformed by the shear flow, stretching in the x-direction, shrinking in the z-direction (and to a lesser extent also shrinking in the y-direction; see Supporting Information), and developing an anisotropic tilt, which signals the presence of shear stress.[61] Another possible extension to eq 20b could be a Gaussian shape:

$$\frac{\langle z\rangle}{\lambda} = 4.3\ \exp\left[-\left(\frac{\langle x\rangle}{22.4\lambda}\right)^2\right] + 4.0 \tag{22}$$

which was used to fit the simulation data in Figure 4b. This function also shrinks quadratically at small shear rates, $\langle \Delta z\rangle \propto -\langle x\rangle^2$, and saturates to $\langle z\rangle \to$ const at very large shear rates, but without a proper theory both eqs 21 or 22 are just guesses. Actually, the simple theoretical eq 20a predicts that the $\langle x\rangle$ displacement will reach a maximum at $\dot{\gamma}\tau_d = 1$ and then slowly retract to zero. The simulation data in Figure 4b clearly rules out this possibility, instead showing that the $\langle x\rangle$ displacement always grows monotonically and eventually saturates to some fixed value.

DISCUSSION

At short time scales the brush behaves like a liquid, while at very long time scales like an elastic solid. The grafted chains of length N relax primarily by the arm retraction mechanism[62] $\tau_a = O(N^3 e^{N/N_e})$. This characteristic time may be further slowed[52] to $\tau_a = O(P^3N^2e^{N/N_e})$ during interdigitation with an entangled bulk polymer of length P. These very slow brush−brush relaxation processes do not couple easily to a transverse shear flow: the bristles are immobilized and cannot flow past each other. An applied shear flow only tilts the entire brush structure including its internal topological arrangements but does not interfere with the inner brush−brush dynamics. The truly interesting coupling is between the brush and the bulk chains. These flow past each other, and therefore the brush−bulk overlap region should show similar behaviors to those of the pure bulk fluid, including shear thinning and normal stress differences, expected to occur at a time scale $\tau_d = O(P^3)$ dictated by the reptation of the free chains, which should overwhelm the slower arm retraction of the brush.

The structural change observed by NR occurs almost instantly upon switching on the shear for both brush-LS and brush-SD, suggesting that the brush−bulk dynamics are governed by a relaxation process faster than the NR time resolution (about 1 min) and therefore consistent with reptation dynamics $\tau_d \approx 1$ s. Overall, the brush−bulk relaxation is too fast to measure with our current setup, and the upper limit is about 1 min. More information on the kinetics of the brush may be obtained in the future, using an oscillatory shear flow combined with stroboscopic NR.[63] If arm retraction of the brush was to play a role, the relaxation time should be exponentially e^{N/N_e} longer and very much different for the two brushes: $\tau_{LS}/\tau_{SD} = (N_{LS}/N_{SD})^3 e^{(N_{LS}-N_{SD})/N_e} \approx 100$. In our experiment we could not detect any difference in the dynamics of the two brushes and therefore conclude that the effect of coupling to shear flow is governed by the free chain reptation, not by the brush itself. This conclusion is corroborated by the fact that the relative brush collapse of both experimental systems and the simulation fall onto a master curve (see Figure 3) in spite of the different grafting densities and chain lengths of the three systems.

We emphasize that the universality of the brush collapse refers only to the brush−-bulk overlap region and does not take into account the interior brush region, which was shown here (Figure 2d) not to couple to the transverse shear flow, at least for the experimentally accessible shear rates. In fact, for very dense brushes the overlap region becomes too narrow to entangle with the bulk chains, in which case we could not observe any NR signal change upon shear (data not shown). We can say that the saturation parameter in eq 21 becomes $\alpha = 1$, meaning that for these very dense brushes the overlap region is already fully collapsed even at shear rate $\dot{\gamma} = 0$.

One important parameter range that we have not explored is when the grafted chains are much longer than the free chains $N \gg P$, and the grafting density is sufficiently low so that more than one free chain can entangle with every grafted chain. In such a scenario the concentration of the brush is too faint to be detected by NR, at least with our present setup. Regardless of neutrons, it may happen for this system that the brush starts collapsing at $Wi \ll 1$, much sooner than the shear-thinning can erode the viscosity of the bulk liquid. If this is the case, then it may be possible[64] that the liquid loses grip with the surface and displays a large shear-dependent surface slip. In all the cases that we studied, $N \lesssim P$, brush collapse happens at the same time as the shear thinning in the bulk, which prevents a large slip from occurring. So far it has not been possible to characterize an appropriate $N \gg P$ system, and the surface slip question remains open.

In summary, we have used a combination of *in situ* rheo-neutron reflectometry, coarse-grained computer simulations, and phenomenological theory to show that it is possible to engineer polymer brushes responding to shear stimuli exerted by an entangled polymer solution. At the same time we provide strong evidence that the time scale of this shear response is governed by the solution dynamics, which sets a clear limit on the tailoring of the shear response of polymer brushes.

ASSOCIATED CONTENT

Supporting Information

The Supporting Information is available free of charge on the ACS Publications website at DOI: 10.1021/acs.macromol.6b02525.

(1) Physical characterization of polymer brushes: NR data in air, in deuterated toluene, and in 10% hPS + 20% dPS polymer solution; (2) reproducibility of the NR measurement under shear; (3) chemical characterization of the brush (FTIR spectrum); (4) rheological characterization of the bulk entangled polymer solution; (5) simulation data of the brush structure under shear (PDF)

AUTHOR INFORMATION

Corresponding Authors

*E-mail: korolkovas@ill.fr (A.K.).
*E-mail: gutfreund@ill.fr (P.G.).

ORCID

Airidas Korolkovas: 0000-0001-7904-5639
Cesar Rodriguez-Emmenegger: 0000-0003-0745-0840
Andres de los Santos Pereira: 0000-0002-0138-1357

Author Contributions

The experiment was designed by M.W., P.G., A.K., and F.R. The "grafting-to" brush was made by A.C. and F.R. The "grafting-from" brush was made by A.S.P. and C.R.E. with participation of A.K. Rheo-NR data were collected and analyzed by P.G. and A.K. with participation of M.W., A.C., and F.A. Simulations and theory were performed by A.K. The manuscript was written by A.K. with the contribution of all authors.

Notes

The authors declare no competing financial interest.

■ ACKNOWLEDGMENTS

The authors thank Jean-Louis Barrat and Lilliane Léger for their invaluable comments and help. We also acknowledge the use of the Partnership for Soft Condensed Matter (PSCM) facilities and the ILL for according beam time.

■ REFERENCES

(1) Milner, S. T. Polymer Brushes. *Science* **1991**, *251*, 905−914.
(2) Brittain, W. J.; Minko, S. A structural definition of polymer brushes. *J. Polym. Sci., Part A: Polym. Chem.* **2007**, *45*, 3505−3512.
(3) Schöttler, S.; Becker, G.; Winzen, S.; Steinbach, T.; Mohr, K.; Landfester, K.; Mailänder, V.; Wurm, F. R. Protein adsorption is required for stealth effect of poly (ethylene glycol)-and poly (phosphoester)-coated nanocarriers. *Nat. Nanotechnol.* **2016**, *11*, 372−377.
(4) Butcher, N. J.; Mortimer, G. M.; Minchin, R. F. Drug delivery: Unravelling the stealth effect. *Nat. Nanotechnol.* **2016**, *11*, 310.
(5) Azzaroni, O. Polymer brushes here, there, and everywhere: Recent advances in their practical applications and emerging opportunities in multiple research fields. *J. Polym. Sci., Part A: Polym. Chem.* **2012**, *50*, 3225−3258.
(6) Bauer, M.; Kekicheff, P.; Iss, J.; Fajolles, C.; Charitat, T.; Daillant, J.; Marques, C. M. Sliding tethered ligands add topological interactions to the toolbox of ligand-receptor design. *Nat. Commun.* **2015**, *6*, 8117.
(7) Raviv, U.; Giasson, S.; Kampf, N.; Gohy, J.-F.; Jérôme, R.; Klein, J. Lubrication by charged polymers. *Nature* **2003**, *425*, 163−165.
(8) Klein, J. Repair or Replacement−A Joint Perspective. *Science* **2009**, *323*, 47−48.
(9) Yang, H.; Esteves, A. C. C.; Zhu, H.; Wang, D.; Xin, J. H. In-situ study of the structure and dynamics of thermo-responsive PNIPAAm grafted on a cotton fabric. *Polymer* **2012**, *53*, 3577−3586.
(10) Pinto, J.; Whiting, G.; Khodabakhsh, S.; Torre, L.; Rodríguez, A.; Dalgliesh, R.; Higgins, A.; Andreasen, J.; Nielsen, M.; Geoghegan, M.; Huck, W.; Sirringhaus, H. Organic Thin Film Transistors with Polymer Brush Gate Dielectrics Synthesized by Atom Transfer Radical Polymerization. *Adv. Funct. Mater.* **2008**, *18*, 36−43.
(11) Youm, S. G.; Hwang, E.; Chavez, C. A.; Li, X.; Chatterjee, S.; Lusker, K. L.; Lu, L.; Strzalka, J.; Ankner, J. F.; Losovyj, Y.; Garno, J. C.; Nesterov, E. E. Polythiophene Thin Films by Surface-Initiated Polymerization: Mechanistic and Structural Studies. *Chem. Mater.* **2016**, *28*, 4787−4804.
(12) Reinhardt, M.; Dzubiella, J.; Trapp, M.; Gutfreund, P.; Kreuzer, M.; Gröschel, A. H.; Müller, A. H. E.; Ballauff, M.; Steitz, R. Fine-Tuning the Structure of Stimuli-Responsive Polymer Films by Hydrostatic Pressure and Temperature. *Macromolecules* **2013**, *46*, 6541−6547.
(13) Brown, A. A.; Azzaroni, O.; Huck, W. T. S. Photoresponsive Polymer Brushes for Hydrophilic Patterning. *Langmuir* **2009**, *25*, 1744−1749.
(14) Lutz, J.-F. Thermo-Switchable Materials Prepared Using the OEGMA-Platform. *Adv. Mater.* **2011**, *23*, 2237−2243.
(15) Tokareva, I.; Minko, S.; Fendler, J. H.; Hutter, E. Nanosensors based on responsive polymer brushes and gold nanoparticle enhanced transmission surface plasmon resonance spectroscopy. *J. Am. Chem. Soc.* **2004**, *126*, 15950−15951.
(16) Stuart, M. A. C.; Huck, W. T. S.; Genzer, J.; Mueller, M.; Ober, C.; Stamm, M.; Sukhorukov, G. B.; Szleifer, I.; Tsukruk, V. V.; Urban, M.; Winnik, F.; Zauscher, S.; Luzinov, I.; Minko, S. Emerging applications of stimuli-responsive polymer materials. *Nat. Mater.* **2010**, *9*, 101−113.
(17) Milner, S.; Witten, T.; Cates, M. Theory of the grafted polymer brush. *Macromolecules* **1988**, *21*, 2610−2619.
(18) Murat, M.; Grest, G. S. Interaction between grafted polymeric brushes: A molecular-dynamics study. *Phys. Rev. Lett.* **1989**, *63*, 1074.
(19) Binder, K.; Milchev, A. Polymer brushes on flat and curved surfaces: How computer simulations can help to test theories and to interpret experiments. *J. Polym. Sci., Part B: Polym. Phys.* **2012**, *50*, 1515−1555.
(20) Kelley, T. W.; Schorr, P. A.; Johnson, K. D.; Tirrell, M.; Frisbie, C. D. Direct force measurements at polymer brush surfaces by atomic force microscopy. *Macromolecules* **1998**, *31*, 4297−4300.
(21) Jones, R. A.; Richards, R. W. *Polymers at Surfaces and Interfaces*; Cambridge University Press: 1999.
(22) Currie, E.; Norde, W.; Cohen Stuart, M. A. Tethered polymer chains: surface chemistry and their impact on colloidal and surface properties. *Adv. Colloid Interface Sci.* **2003**, *100−102*, 205−265.
(23) Kato, K.; Uchida, E.; Kang, E.-T.; Uyama, Y.; Ikada, Y. Polymer surface with graft chains. *Prog. Polym. Sci.* **2003**, *28*, 209−259.
(24) Malham, I. B.; Bureau, L. Density effects on collapse, compression, and adhesion of thermoresponsive polymer brushes. *Langmuir* **2010**, *26*, 4762−4768.
(25) La Spina, R.; Tomlinson, M. R.; Ruiz-Pérez, L.; Chiche, A.; Langridge, S.; Geoghegan, M. Controlling network-brush interactions to achieve switchable adhesion. *Angew. Chem., Int. Ed.* **2007**, *46*, 6460−6463.
(26) Durliat, E.; Hervet, H.; Leger, L. Influence of grafting density on wall slip of a polymer melt on a polymer brush. *Europhys. Lett.* **1997**, *38*, 383.
(27) Léger, L.; Raphal, E.; Hervet, H. *Polymers in Confined Environments*; Adv. Polymer Sci.; Springer: 1999; Vol. *138*, pp 185−225.
(28) Cohen, C.; Restagno, F.; Poulard, C.; Leger, L. Incidence of the molecular organization on friction at soft polymer interfaces. *Soft Matter* **2011**, *7*, 8535−8541.
(29) Thorsen, T.; Maerkl, S.; Quake, S. Microfluidic large-scale integration. *Science* **2002**, *298*, 580−584.
(30) Raviv, U.; Giasson, S.; Kampf, N.; Gohy, J.-F.; Jerome, R.; Klein, J. Lubrication by charged polymers. *Nature* **2003**, *425*, 163−165.
(31) Larson, R. G.; Desai, P. S. Modeling the rheology of polymer melts and solutions. *Annu. Rev. Fluid Mech.* **2015**, *47*, 47−65.
(32) Korolkovas, A.; Gutfreund, P.; Barrat, J.-L. Simulation of Entangled Polymer Solutions. *J. Chem. Phys.* **2016**, *145*, 124113.
(33) Wolff, M.; Kuhns, P.; Liesche, G.; Ankner, J. F.; Browning, J. F.; Gutfreund, P. Combined neutron reflectometry and rheology. *J. Appl. Crystallogr.* **2013**, *46*, 1729−1733.
(34) Grest, G. S. *Polymers in Confined Environments*; Springer: 1999; pp 149−183.
(35) Binder, K.; Kreer, T.; Milchev, A. Polymer brushes under flow and in other out-of-equilibrium conditions. *Soft Matter* **2011**, *7*, 7159−7172.
(36) Müller, M.; Pastorino, C. Cyclic motion and inversion of surface flow direction in a dense polymer brush under shear. *EPL (Europhysics Letters)* **2008**, *81*, 28002.
(37) Singh, M. K.; Ilg, P.; Espinosa-Marzal, R. M.; Kröger, M.; Spencer, N. D. Polymer Brushes under Shear: Molecular Dynamics Simulations Compared to Experiments. *Langmuir* **2015**, *31*, 4798−4805.
(38) Mendonça, A. C.; Goujon, F.; Malfreyt, P.; Tildesley, D. J. Monte Carlo simulations of the static friction between two grafted polymer brushes. *Phys. Chem. Chem. Phys.* **2016**, *18*, 6164−6174.
(39) Pastorino, C.; Binder, K.; Kreer, T.; Müller, M. Static and dynamic properties of the interface between a polymer brush and a melt of identical chains. *J. Chem. Phys.* **2006**, *124*, 064902.
(40) Römer, F.; Fedosov, D. Dense brushes of stiff polymers or filaments in fluid flow. *EPL (Europhysics Letters)* **2015**, *109*, 68001.
(41) Saphiannikova, M. G.; Pryamitsyn, V. A.; Cosgrove, T. Self-consistent Brownian dynamics simulation of polymer brushes under shear. *Macromolecules* **1998**, *31*, 6662−6668.
(42) de Gennes, P. G. *Scaling Concepts in Polymer Physics*; Cornell University Press: 1979.
(43) Bolhuis, P.; Louis, A.; Hansen, J.; Meijer, E. Accurate effective pair potentials for polymer solutions. *J. Chem. Phys.* **2001**, *114*, 4296−4311.
(44) Nikunen, P.; Vattulainen, I.; Karttunen, M. Reptational dynamics in dissipative particle dynamics simulations of polymer melts. *Phys. Rev. E* **2007**, *75*, 036713.

(45) Baker, S. M.; Smith, G. S.; Anastassopoulos, D. L.; Toprakcioglu, C.; Vradis, A. A.; Bucknall, D. G. Structure of Polymer Brushes under Shear Flow in a Good Solvent. *Macromolecules* **2000**, *33*, 1120−1122.
(46) Ivkov, R.; Butler, P. D.; Satija, S. K.; Fetters, L. J. Effect of Solvent Flow on a Polymer Brush: A Neutron Reflectivity Study of the Brush Height and Chain Density Profile. *Langmuir* **2001**, *17*, 2999−3005.
(47) Sasa, L. A.; Yearley, E. J.; Jablin, M. S.; Gilbertson, R. D.; Lavine, A. S.; Majewski, J.; Hjelm, R. P. Shear-induced metastable states of end-grafted polystyrene. *Phys. Rev. E* **2011**, *84*, 021803.
(48) Wolff, M.; Gutfreund, P.; Rühm, A.; Akgun, B.; Zabel, H. Nanoscale discontinuities at the boundary of flowing liquids: a look into structure. *J. Phys.: Condens. Matter* **2011**, *23*, 184102.
(49) Chennevière, A.; Cousin, F.; Boué, F.; Drockenmuller, E.; Shull, K. R.; Léger, L.; Restagno, F. Direct Molecular Evidence of the Origin of Slip of Polymer Melts on Grafted Brushes. *Macromolecules* **2016**, *49*, 2348−2353.
(50) Weissenberg, K. A continuum theory of rheological phenomena. *Nature* **1947**, *159*, 310−311.
(51) Rodriguez-Emmenegger, C.; Janel, S.; de los Santos Pereira, A.; Bruns, M.; Lafont, F. Quantifying bacterial adhesion on antifouling polymer brushes via single-cell force spectroscopy. *Polym. Chem.* **2015**, *6*, 5740−5751.
(52) Chennevière, A.; Drockenmuller, E.; Damiron, D.; Cousin, F.; Boué, F.; Restagno, F.; Léger, L. Quantitative Analysis of Interdigitation Kinetics between a Polymer Melt and a Polymer Brush. *Macromolecules* **2013**, *46*, 6955−6962.
(53) Ell, J. R.; Mulder, D. E.; Faller, R.; Patten, T. E.; Kuhl, T. L. Structural determination of high density, ATRP grown polystyrene brushes by neutron reflectivity. *Macromolecules* **2009**, *42*, 9523−9527.
(54) Campbell, R.; Wacklin, H.; Sutton, I.; Cubitt, R.; Fragneto, G. FIGARO: The new horizontal neutron reflectometer at the ILL. *Eur. Phys. J. Plus* **2011**, *126*, 107.
(55) Gay, C. Wetting of a polymer brush by a chemically identical polymer melt. *Macromolecules* **1997**, *30*, 5939−5943.
(56) Korolkovas, A. Simulating confined particles with a flat density profile. *Phys. Rev. E: Stat. Phys., Plasmas, Fluids, Relat. Interdiscip. Top.* **2016**, *94*, 021302.
(57) Karim, A.; Satija, S. K.; Douglas, J. F.; Ankner, J. F.; Fetters, L. J. Neutron Reflectivity Study of the Density Profile of a Model End-Grafted Polymer Brush: Influence of Solvent Quality. *Phys. Rev. Lett.* **1994**, *73*, 3407−3410.
(58) Leibler, L.; Ajdari, A.; Mourran, A.; Coulon, G.; Chatenay, D. *Ordering in Macromolecular Systems*; Springer: 1994; pp 301−311.
(59) Karayiannis, N. C.; Kröger, M. Combined molecular algorithms for the generation, equilibration and topological analysis of entangled polymers: Methodology and performance. *Int. J. Mol. Sci.* **2009**, *10*, 5054−5089.
(60) Kreer, T. Polymer-brush lubrication: a review of recent theoretical advances. *Soft Matter* **2016**, *12*, 3479−3501.
(61) Janeschitz-Kriegl, H. *Polymer Melt Rheology and Flow Birefringence*; Springer Science & Business Media: 2012; Vol. *6*.
(62) Lang, M.; Werner, M.; Dockhorn, R.; Kreer, T. Arm Retraction Dynamics in Dense Polymer Brushes. *Macromolecules* **2016**, *49*, 5190−5201.
(63) Adlmann, F. A.; Gutfreund, P.; Ankner, J.; Browning, J.; Parizzi, A.; Vacaliuc, B.; Halbert, C.; Rich, J.; Dennison, A.; Wolff, M. Towards neutron scattering experiments with sub-millisecond time resolution. *J. Appl. Crystallogr.* **2015**, *48*, 220−226.
(64) Brochard, F.; De Gennes, P. G. Shear-dependent slippage at a polymer/solid interface. *Langmuir* **1992**, *8*, 3033−3037.